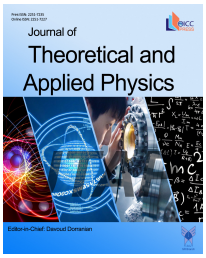

Volume 18, Issue 6, 182478 (1-12)

Journal of Theoretical and Applied Physics (JTAP)

https://dx.doi.org/10.57647/j.jtap.2024.1806.78

Assessment of a compressible lattice Boltzmann method in analyzing shock wave/boundary layer interaction in a supersonic inlet

Hiwa Hosseini*, Ebrahim Goshtasbi Rad

Aerospace Division, Department of Mechanical Engineering, Shiraz University, Shiraz, Iran.

***Corresponding author:** hosseini.hiwa@gmail.com

Original Research

Received:
24 September 2024
Revised:
26 October 2024
Accepted:
4 November 2024
Published online:
30 December 2024

Abstract:

The double distribution function lattice Boltzmann method (DDF LBM) has been explored for its potential applications in a supersonic inlet. The goal is to evaluate its ability to estimate the physics of shock wave/boundary layer interaction (SWBLI), including shock formation and separation bubble size. To validate the stability characteristics of DDF LBM, authors studied a well-known benchmark problem-the shock tube and the compressible flow around an airfoil. This involved calculating the propagation of normal and oblique shocks and predicting the location of contact discontinuities. Subsequently, the method was tested to predict the physics of shock wave and boundary layer interaction near a supersonic inlet. Notably, accurate predictions require careful consideration of space discretization, proper selection of the Courant-Friedrichs-Lewy (CFL) number, and parameter adjustments. Two discretization schemes-the fifth-order weighted essentially non-oscillatory (WENO) and the third-order weighted non-free-parameter dissipation (WNND) schemes-were assessed for their effectiveness in capturing the relevant physics.

Keywords: Lattice Boltzmann method; Compressible flow; Shock wave/boundary layer interaction

1. Introduction

The interaction between shock waves and the boundary layer on a surface is a fundamental challenge in fluid mechanics. Researchers encounter this phenomenon in various contexts, such as estimating loads on nozzle walls in rocket propulsion studies. In these scenarios, issues like viscous flow with positive pressure gradients, flow separation due to shock formation, shear layers, and rotating flow separation bubbles must be addressed. For instance, supersonic aircraft experience shock waves formed at the engine inlet, which transition the flow from supersonic to subsonic as it enters the engine. Accurately predicting the flow physics in such situations falls under the category of shock wave-boundary layer interaction (SWBLI).

A comprehensive study by Dolling in 2001 [1] reviewed research on shock wave-boundary layer interaction over the past 50 years. Despite significant advancements in numerical methods and experimental studies, challenges remain. Issues like overestimated temperature rise and unsteady pressure loads persist. While the author remains optimistic about future research, limitations related to time, cost, and complex aerial missions necessitate a precise understanding of the physics and accurate simulation results.

Over the past three decades, the lattice Boltzmann method (LBM) has captivated the research community and academic scholars. Its appeal lies in its simplicity, suitability for parallel systems, and ability to model intricate geometries. The method is grounded in the robust Boltzmann equation. Notably, well-established approaches, including the Chapman-Enskog expansion, connect dynamic conditions in LBM to conservation equations on a macroscopic scale. Functioning as a bridge between microscopic and macroscopic realms, the recently developed lattice Boltzmann method operates in the mesoscopic domain, capturing essential features of fluid flow problems. Although its origins trace back to lattice gas automata, its current form emerges from discretizing the renowned Boltzmann equation. This discretization occurs in the velocity domain, alongside spatial and temporal discretizations, accounting for finite velocity values within

each LBM framework. Given that the Boltzmann equation encompasses all necessary physics, LBM finds application across a wide range of computational fluid dynamics problems.

In the 2000s, the compressible version of the lattice Boltzmann method (LBM) was introduced and has since evolved. Three main categories are considered: multispeed, double distribution function (DDF), and hybrid methods.

Multispeed Methods: These extend isothermal models by using a greater number of discrete velocities to account for compressibility effects. In these models, the equilibrium distribution function, f_i^{eq}, includes higher-order terms of particle velocity to properly recover the energy equation. However, multispeed methods suffer from numerical instability, and temperature variation is limited.

Double distribution function (DDF) models: DDF introduces a new distribution function for energy, separate from the density distribution function. Pressure and velocity are still estimated using the standard LBM. In the absence of viscous heat dissipation and compression work, temperature can be treated as a scalar transported by the velocity field. DDF models are more stable than multispeed methods and cover a wider temperature range.

Hybrid methods: These resolve continuity and momentum using LBM while handling energy using other approaches (e.g., finite difference or finite volume methods). Hybrid methods have fewer distribution functions compared to multispeed and DDF methods, resulting in better performance.

In a 2008 PhD dissertation, Kun [2] introduced a novel lattice Boltzmann (LB) model and corresponding equilibrium distribution functions for simulating compressible flows. Instead of the complex Maxwell equation, this study replaces it with a simpler equilibrium function that satisfies the necessary relations to recover the Navier-Stokes (NS) equations. To distribute this function across lattice sites in velocity space, Lagrangian interpolation is employed. Using this approach, several models are developed for compressible/incompressible and viscous/inviscid flows. The discrete Boltzmann equation is solved using the finite volume method, which effectively models shock waves and other discontinuities at high Mach numbers. Additionally, various boundary conditions (such as slip/no-slip on walls) are considered. The proposed models and solution method are validated against existing literature results. Numerical investigations demonstrate that this method can simulate flows at Mach 10.

In 2012, Xu et al. [3] reviewed their group's research on compressible lattice Boltzmann methods. The main categories include single relaxation time LBM with an extra viscosity term, multiple relaxation time models, and investigations into hydrodynamic instabilities. These instabilities, common in natural and industrial processes, are classified into three main types: RT, RM, and KH instabilities.

In 2014, Li and Zhang [4] conducted a study on compressible flows using the lattice Boltzmann method (LBM). Their approach, based on a multispeed lattice, introduced an additional distribution function to account for potential energy and recover the Navier-Stokes (NS) equations. The Chapman-Enskog expansion was employed to derive the equilibrium density distribution function in two dimensions with 17 discrete velocities. Equations were discretized using a third-order upwind scheme, and the von Albada limiter was used to prevent unwanted fluctuations. Validation involved simulating the Riemann problem, Couette flow, and NACA0012 airfoil, with detailed initial conditions and specifications.

Li et al. [5] introduced a well-known double distribution function in 2007, based on a circular function to extract the equilibrium distribution. This DDF approach was chosen by the authors to simulate shock and boundary layer interaction at the entrance of a diffuser in supersonic flows. Initially validated against the benchmark shock tube problem, it was then applied to 2-dimensional problems, evaluating its capabilities for compressible viscous flows-especially those involving shock waves and boundary layers, which exhibit intriguing features.

In 2017, Qiu et al. [6] utilized the double distribution function LB model proposed by Li et al. [5] to simulate compressible viscous flows. They successfully solved the Riemann problem and Couette flow for validation. Subsequently, they simulated three cases: a compressible boundary layer, a shock wave, and the shock wave/boundary layer interaction. Laminar supersonic flow over an insulated flat plate at Mach numbers 2, 4, and 6 was modeled to investigate the numerical results.

In their research, Jammalamadka et al. [7] investigated the canonical shock wave-boundary layer interaction (SWBLI) problem using an LBM-VLES (Large Eddy Simulation) approach. Their simulations were conducted in three dimensions (3D) and were unsteady, focusing on a Mach number of 1.7. They employed the commercial software PowerFLOW for their investigations, utilizing variable refinement regions to enhance grid size. Turbulence initiation was achieved using a zig-zag strip. Notably, their findings revealed an anti-correlation between temperature and velocity fields—increasing one led to a decrease in the other. Additionally, vortical structures were visualized in 3D, and the results from 2D and 3D simulations closely matched. Furthermore, low-frequency oscillations in the shock system were captured.

Another significant study by Qiu et al. [8] explored non-equilibrium effects in a shock tube. They assessed the hydrodynamic and thermodynamic impacts of shock waves, contact discontinuities, and rarefaction waves. Using a mesoscopic kinetic approach with detailed molecular velocity distribution descriptions, they examined the physical significance of kinetic moments in a one-dimensional shock tube problem. Their conclusions highlighted that non-equilibrium effects are more pronounced in shock waves compared to contact discontinuities and rarefaction waves. Interestingly, despite their strength, non-equilibrium effects in shock waves are not stable. Interaction with the contact discontinuity alters the direction of these effects, while interacting rarefaction waves result in sharp crests in most non-equilibrium kinetic moments.

The objective of this study is to evaluate the performance of a double-distribution-function-based lattice Boltzmann method (DDF-LBM) in capturing the underlying physics

of shock wave boundary layer interaction (SWBLI). To achieve this, we validate the DDF-LBM using well-known benchmark problems: the compressible shock tube problem in both 1D and 2D, as well as a 2D airfoil flow. Subsequently, we apply the method to a 2D supersonic inlet and compare its results with those obtained by Soltani et al. [9].

2. Methodology

Double distribution function methods are evolved upon the fact that the energy needs a separate distribution function to be coupled with the density distribution function via the equation of state and acts as a serious alternative for conventional CFD methods in solving Navier-Stokes equations. Accordingly, there will be another equilibrium distribution function for energy. The method by Li et al. [5] is introduced as follows:
The following equations should be solved for density and energy distribution functions:

$$\frac{\partial f_i}{\partial t}+\mathbf{e_i}\cdot\nabla f_i=-\frac{1}{\tau_f}(f_i-f_i^{eq}) \tag{1}$$

$$\frac{\partial h_i}{\partial t}+\mathbf{e_i}\cdot\nabla h_i=-\frac{1}{\tau_h}(h_i-h_i^{eq})+\frac{\mathbf{e_i}\cdot u}{\tau_{hf}}(f_i-f_i^{eq}) \tag{2}$$

where f_i and h_i are density and energy distribution functions, respectively with their corresponding equilibrium distribution functions f_i^{eq} and h_i^{eq}. $\mathbf{e_i}$ is discrete velocity and τ_f and τ_h are relaxation times for density and energy, respectively. In which $\tau_{hf}=\tau_h\tau_f/(\tau_f-\tau_h)$.
The velocity set is defined as:

$$\frac{\mathbf{e_i}}{\sqrt{RT_c}}=\begin{cases}(0,0), & i=0\\ cyc:(\pm1,0), & i=1,2,3,4\\ cyc:\sqrt{2}(\pm1,\pm1), & i=5,6,7,8\\ cyc:2(\pm1,0), & i=9,10,11,12.\end{cases} \tag{3}$$

By use of the Chapman-Enskog expansion, Navier-Stokes equations are derived as:

$$\frac{\partial\rho}{\partial t}+\frac{\partial\rho u_\alpha}{\partial x_\alpha}=0 \tag{4}$$

$$\frac{\partial\rho u_\alpha}{\partial t}+\frac{\partial\rho u_\alpha u_\beta}{\partial x_\beta}+\frac{\partial p}{\partial x_\alpha}=\frac{\partial \acute{P}_{\alpha\beta}}{\partial x_\beta} \tag{5}$$

$$\frac{\partial\rho E}{\partial t}+\frac{\partial(\rho E+p)u_\alpha}{\partial x_\alpha}=\frac{\partial}{\partial x_\beta}(\lambda\frac{\partial T}{\partial x_\beta}+\acute{P}_{\alpha\beta}u_\alpha) \tag{6}$$

where

$$p=\rho RT,\ \text{and}$$
$$\acute{P}_{\alpha\beta}=\mu\left(\frac{\partial u_\alpha}{\partial x_\beta}+\frac{\partial u_\beta}{\partial x_\alpha}-\frac{2}{D}\frac{\partial u_\chi}{\partial x_\chi}\delta_{\alpha\beta}\right)$$

Parameters in Equation (6) are defined as follows:

$$\mu=\tau_f p,\ \ \mu_B=(\frac{2}{D}-\frac{2}{b})\tau_f p,\ \ \lambda=\tau_h c_p p \tag{7}$$

Macroscopic variables are obtained by the following relations:

$$\rho=\sum_i f_i,\ \ u=\sum_i f_i\frac{\mathbf{e_i}}{\rho},\ \ T=2\frac{\sum_i\frac{h_i}{\rho}-\frac{|u|^2}{2}}{bR} \tag{8}$$

Within the compressible lattice Boltzmann (LB) community, researchers commonly employ the IMEX-RK scheme for time discretization. When it comes to space discretization, scholars often favor various versions of weighted nonnegative distribution (WNND) and fifth-order Weighted Essentially Non-Oscillatory (WENO) schemes. In our current study, we follow the approach proposed by Qiu et al. [8], where we specifically utilize the Z version of the third-order WNND (WNND-Z) to enhance the numerical performance of the compressible double-distribution-function lattice Boltzmann method (DDF-LBM). Both WNND and WENO schemes offer advantages in simulating flow discontinuities, and their convergence capabilities are superior.
More details regarding the equilibrium distribution functions as well as the second-order Implicit Explicit (IMEX) Runge-Kutta method are outlined in [5]. Based on the above-mentioned reasoning, two different schemes are considered for spatial discretization. The fifth-order WENO scheme with a 7-point stencil and the third-order WNND scheme with a 5-point stencil. In the WENO scheme, the convective term is defined as follows: $e_{\alpha x}f_{\alpha,I,J}$

$$\frac{\partial e_{\alpha x}f_{\alpha,I,J}}{\partial x}=\frac{1}{\Delta x}(\hat{F}_{\alpha,I+1/2,J}-\hat{F}_{\alpha,I-1/2,J}) \tag{9}$$

where $e_{\alpha x}$ is the x component of e_α, $\hat{F}_{\alpha,I+1/2,J}$ is the numerical flux at the interface of $x_I+\Delta x/2$ which is defined as:

$$\hat{F}_{\alpha,I+1/2,J}=w_1\hat{F}^1_{\alpha,I+1/2,J}+w_2\hat{F}^2_{\alpha,I+1/2,J}+w_3\hat{F}^3_{\alpha,I+1/2,J} \tag{10}$$

Under condition $e_{\alpha x}\geq 0$, these three fluxes are given by:

$$\hat{F}^1_{0,\alpha,I+1/2,J}=\frac{1}{3}\hat{F}_{\alpha,I-2,J}-\frac{7}{6}F_{\alpha,I-1,J}+\frac{11}{6}F_{\alpha,I,J} \tag{11}$$

$$\hat{F}^2_{0,\alpha,I+1/2,J}=-\frac{1}{6}F_{\alpha,I-1,J}+\frac{5}{6}F_{\alpha,I,J}+\frac{1}{3}F_{\alpha,I+1,J} \tag{12}$$

$$\hat{F}^3_{0,\alpha,I+1/2,J}=\frac{1}{3}F_{\alpha,I,J}+\frac{5}{6}F_{\alpha,I+1,J}-\frac{1}{6}F_{\alpha,I+2,J} \tag{13}$$

where $F_{\alpha,I,J}=e_{\alpha x}f_{\alpha,I,J}$.
The weighting factors are given by:

$$w_q=\frac{\tilde{w}_q}{\tilde{w}_1+\tilde{w}_2+\tilde{w}_3} \tag{14}$$

$$\tilde{w}_q=\frac{\delta_q}{(10^{-6}+\sigma_q)^2} \tag{15}$$

with $\delta_1=1/10$, $\delta_2=3/5$, $\delta_3=3/10$. Coefficients σ_qs are smoothness indicators defined by:

$$\sigma_1=\frac{13}{12}(F_{\alpha,I-2,J}-2F_{\alpha,I-1,J}+F_{\alpha,I,J})^2+\frac{1}{4}(F_{\alpha,I-2,J}-4F_{\alpha,I-1,J}+3F_{\alpha,I,J})^2 \tag{16}$$

$$\sigma_2=\frac{13}{12}(F_{\alpha,I-1,J}-2F_{\alpha,I,J}+F_{\alpha,I+1,J})^2+\frac{1}{4}(F_{\alpha,I-1,J}-F_{\alpha,I+1,J})^2 \tag{17}$$

$$\sigma_3 = \frac{13}{12}(F_{\alpha,I,J} - 2F_{\alpha,I+1,J} + F_{\alpha,I+2,J})^2 + \frac{1}{4}(3F_{\alpha,I,J} - 4F_{\alpha,I+1,J} + F_{\alpha,I+2,J})^2 \quad (18)$$

For the WNND scheme:

$$\frac{\partial e_{\alpha x} f_{\alpha,I,J}}{\partial x} = \frac{1}{\Delta x}(\hat{F}_{\alpha,I+1/2,J} - \hat{F}_{\alpha,I-1/2,J}) \quad (19)$$

where $\hat{F}_{\alpha,I+1/2,J}$ is the numerical flux at the interface of $x_I + \Delta x/2$, and given by:

$$\hat{F}_{\alpha,I+1/2,J} = \hat{F}^{+}_{\alpha,I+1/2,J} + \hat{F}^{-}_{\alpha,I+1/2,J} \quad (20)$$

In which $\hat{F}^{+}_{\alpha,I+1/2,J}$ and $\hat{F}^{-}_{\alpha,I+1/2,J}$ are the positive and negative numerical fluxes, respectively. We go through the following just for the positive part since the negative one should be extracted symmetrically.

$$\hat{F}^{+}_{\alpha,I+1/2,J} = \sum_{k=0}^{1} w_k \hat{F}^{+}_{k,\alpha,I+1/2,J} \quad (21)$$

where

$$\hat{F}^{+}_{0,\alpha,I+1/2,J} = -\frac{1}{2}\hat{F}^{+}_{\alpha,I-1,J} + \frac{3}{2}\hat{F}^{+}_{\alpha,I,J}\hat{F}^{+}_{1+\alpha,I+1/2,J} = \frac{1}{2}\hat{F}^{+}_{\alpha,I,J} + \frac{3}{2}\hat{F}^{+}_{\alpha,I+1,J} \quad (22)$$

$\hat{F}^{+}_{\alpha,I,J}$ and $\hat{F}^{-}_{\alpha,I,J}$ are defined as:

$$\hat{F}^{+}_{\alpha,I,J} = \frac{1}{2}(e_{\alpha x} + |e_{\alpha x}|) f_{\alpha,I,J} \quad (23)$$

$$\hat{F}^{-}_{\alpha,I,J} = \frac{1}{2}(e_{\alpha x} - |e_{\alpha x}|) f_{\alpha,I,J} \quad (24)$$

Weights are calculated as:

$$w_k = \frac{\alpha_k}{\sum_{l=0}^{1} \alpha_l}, \quad k = 0,1 \quad (25)$$

In which coefficients α_k are as follows for the WNND-Z scheme:

$$\alpha_k = d_k(1.0 + \frac{\beta_Z}{\mathrm{IS}_k + \varepsilon}), \quad k = 0,1 \quad (26)$$

where d_k are the ideal weights with the values $d_0 = 1/3$ and $d_1 = 2/3$, and the value of ε is 10^{-6}. The expression of IS_k and β_Z are:

$$\mathrm{IS}_0 = (F^{+}_{\alpha,I,J} - F^{-}_{\alpha,I-1,J})^2 \quad (27)$$

$$\mathrm{IS}_1 = (F^{+}_{\alpha,I+1,J} - F^{-}_{\alpha,I,J})^2 \quad (28)$$

$$\beta_Z = \left|\mathrm{IS}_{GZ} - \frac{\mathrm{IS}_0 + \mathrm{IS}_1}{2}\right|, \quad \mathrm{IS}_{GZ} = \frac{1}{4}(F^{+}_{\alpha,I+1,J} - F^{+}_{\alpha,I-1,J})^2 \quad (29)$$

As for the Courant-Friedrichs-Lewy (CFL) number, it must be chosen carefully to ensure thorough capture of flow evolution. The CFL number is defined as: $\mathrm{CFL} = (\Delta t \cdot \max|e_\alpha|)/(\min\{\Delta x, \Delta y\})$. Here, Δt represents the time step, while Δx and Δy correspond to the spatial steps. This number should be small enough for the numerical scheme to capture the whole flow evolution successfully since flow with discontinuities have the potential of numerical instabilities which should be suppressed accordingly. Numerical oscillation near the shock is high so specific care should be taken in selecting the proper value for the CFL number. Achieving stability conditions requires a compromise between these simulation parameters, considering that particle velocity is determined by the model.

3. Validation

Firstly, the method is applied to obtain density and velocity distributions in a shock tube. The shock tube is a benchmark test case to assess the ability of different numerical methods to estimate the behavior of compressible flows. It consists of a diaphragm which divides the tube into two high density and pressure and low density and pressure sides. A 400×5 uniform mesh was considered, and the two ends are walls while we have periodicity in the vertical directions. Initial conditions are as follows.

$$\left(\frac{\rho}{\rho_0}, \frac{u_x}{u_0}, \frac{p}{p_0}\right) = (1,0,1), \quad 0 < \frac{x}{L_0} \leq \frac{1}{2} \quad (30)$$

$$\left(\frac{\rho}{\rho_0}, \frac{u_x}{u_0}, \frac{p}{p_0}\right) = (0.125,0,0.1), \quad \frac{1}{2} < \frac{x}{L_0} \leq 1 \quad (31)$$

When the diaphragm is picked up, a compression wave in the form of a normal shock moves from the high-pressure side to the low-pressure side. An expanding wave is also formed going in the opposite direction to the normal shock. Figure 1 shows an acceptable level of agreement in comparing the results with the exact solution since both the locations of discontinuity and the shock wave are estimated correctly.

In two dimensions, a NACA 0012 airfoil is considered to validate the results of DDF LBM. A 200×200 uniform rectangular mesh with sides equal to 7 chord lengths ($c = 1$) is generated. For upper, lower and left boundaries, equilibrium boundary condition with macroscopic variables are considered while the right boundary is set to be open. Surface of the airfoil is set to be a no-slip wall.

Initial values are set to be $\rho_0 = 1.165$ kg/m^3, $R = 287$ J/(kg.K), $T_0 = 288.15\ K$, $\mu = 1.789e5$ kg/(m.s). The first case was performed for the airfoil at Mach number 0.85 and angle of attack 1 degree and results of two discretization schemes (5$^{\text{th}}$ order WENO and 3$^{\text{rd}}$ order WNND) are compared in Figure 2 to those presented in Figure 4 of [10] by Zhou et al.

According to this figure, results of WENO and WNND schemes match well together and are close to experimental results except for small portions on the lower surface of the airfoil.

For the second case, NACA 0012 airfoil is studied in a flow of with Mach number 0.8, Reynolds number 500 and angle of attack 10 to compare the results with those presented in figure 23 of [11] by Hafez et al. Such a comparison is shown in Figure 3.

As it is evident, pressure values obtained from the WNND scheme are closer to the results of Hafez et al while values from the WENO scheme are slightly higher.

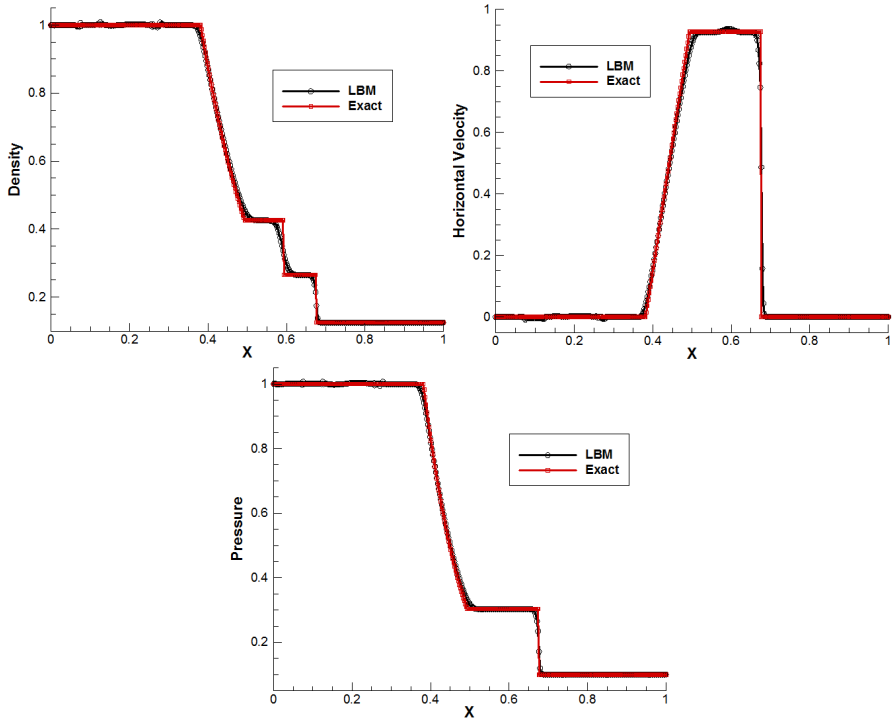

Figure 1. Comparison between the exact solution and results of the DDF LBM for normalized distribution of (a): density (ρ), (b): horizontal velocity (u) and (c): pressure (p) in a shock tube vs. normalized length (x).

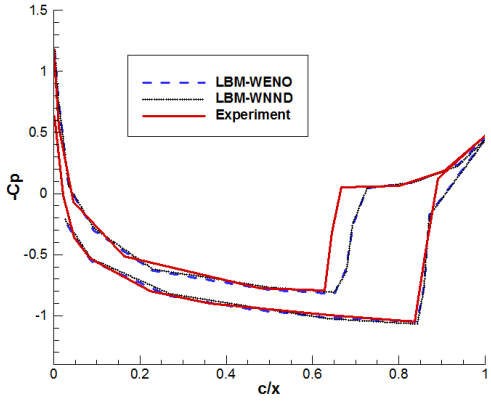

Figure 2. Pressure coefficient on the airfoil surface.

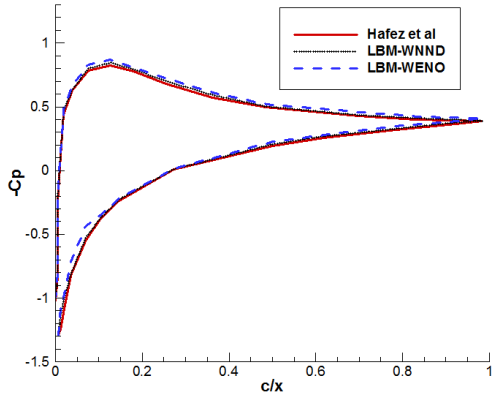

Figure 3. Pressure coefficient on the airfoil body.

The shock tube problem defined in Equations (30) and (31) is considered in two dimensions with a 400×200 mesh using both WNND and WENO schemes. Results are presented in the Figures 4 & 5.

As it can be observed, after 0.1 s the shock front almost has arrived at $x = 0.7$ and there are considerable density changes at the shock foot area for both methods. When the diaphragm is removed, the unsteady process of shock wave/boundary layer interaction starts. In the beginning, the incident contact discontinuity and shock wave move right and interact with the bottom wall of the tube, creating a boundary layer. Then, some vortices are generated due to the boundary layer, resulting in the evolution of complex flow pattern on the bottom wall. The shock wave/boundary layer interaction in the shock tube leads to a lambda-shape like shock pattern.

4. Results and discussion

As the main concentration of this study and based on the study by Soltani et al. [9], a typical two-dimensional geometry of a supersonic inlet is constructed to be studied by the DDF LBM in supersonic airflow. The corresponding geometry is illustrated in Figure 6. A uniform rectangular grid is used in this study and a flow with Mach number 2 and Reynolds number 500 was considered. Other settings for the simulation are as: $\gamma = 1.4$, $Pr = 0.71$, $R = 1$, $\mu = 1/Re$. A C++ program was developed to carry out the computations. Different parts of the problem from the equilibrium to the discretization schemes are all written in separate functions to be called in their appropriate sequence.

Figure 7 shows a comparison between results obtained by three different mesh sizes for density distribution at a speci-

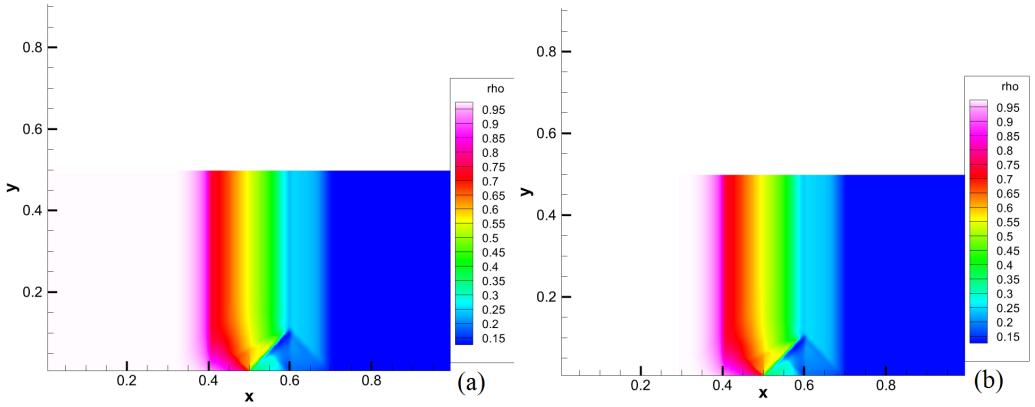

Figure 4. Density distribution in a 2D shock tube problem, (a): WNND scheme, (b): WENO scheme.

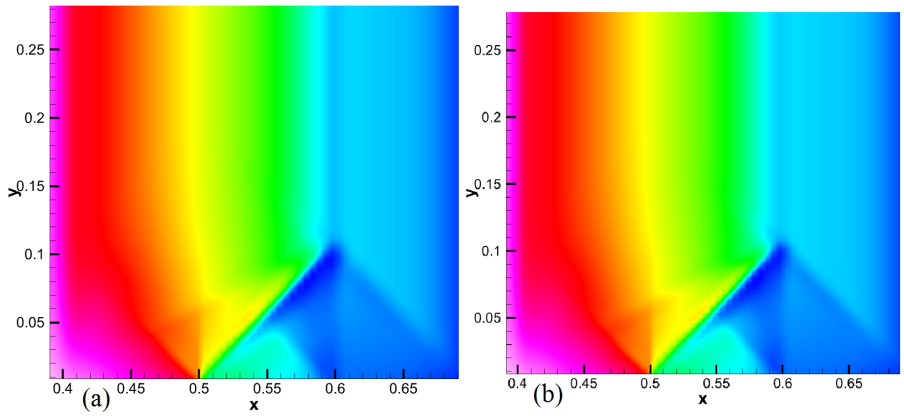

Figure 5. Magnified views of density distribution in a 2D shock tube problem, (a): WNND scheme, (b): WENO scheme.

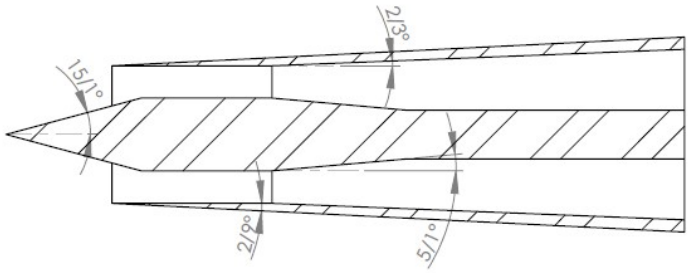

Figure 6. Geometry of the supersonic inlet.

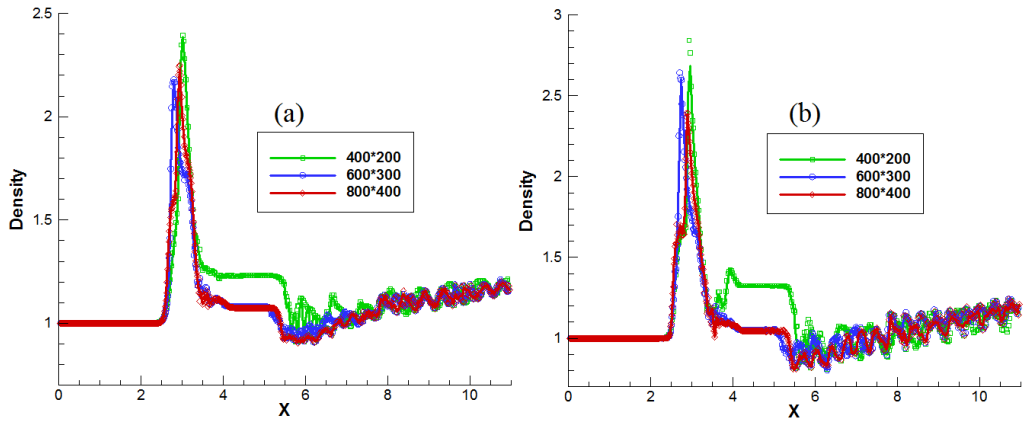

Figure 7. Mesh dependency results (a): WNND, (b): WENO).

Table 1. Results of the mesh dependency study.

Grid sizes	Maximum discrepancy (WNND)	Maximum discrepancy (WENO)
400×200 vs 600×300	10%	12%
400×200 vs 800×400	12%	15%
600×300 vs 800×400	2%	3%

fied y-station ($y = 0.8$).

Three different grid sizes were selected to be tested in the simulations namely, a 400×200, a 600×300 and a 800×400 grid. According to Table 1, results were almost the same but the 600×300 grid was selected for final simulations since it has sufficient resolution, and its computational cost is not as high as the 800×400 one.

A horizontal supersonic flow with Mach number 2 is considered at the left boundary symmetrical with respect to the lower part of the domain. The right and upper boundaries are considered as open boundaries while the surface walls are set to be bounce-back type for which a special function is provided in the flux calculation step. In this function, wall nodes are firstly identified by calling another function and then the no slip bounce back method is applied. Regarding the computational domain, it should be mentioned that a chord length of 1 is considered in our computational code to care for length units, and the computational domain is 11*chord length in the horizontal direction while the vertical direction is half of this value due to symmetric boundary condition. Also, the grid is uniform with equal spatial increments in both directions. Three ghost layers are considered at each boundary.

For the WENO scheme, solution diverges for CFL numbers more than 0.5 while for the WNND scheme gives acceptable results at CFL numbers smaller than 0.7 so a CFL number of 0.5 is selected to get acceptable results by both discretization schemes. Figures 4 and 5 show the contours of density and horizontal velocity for the inlet at its supercritical regime.

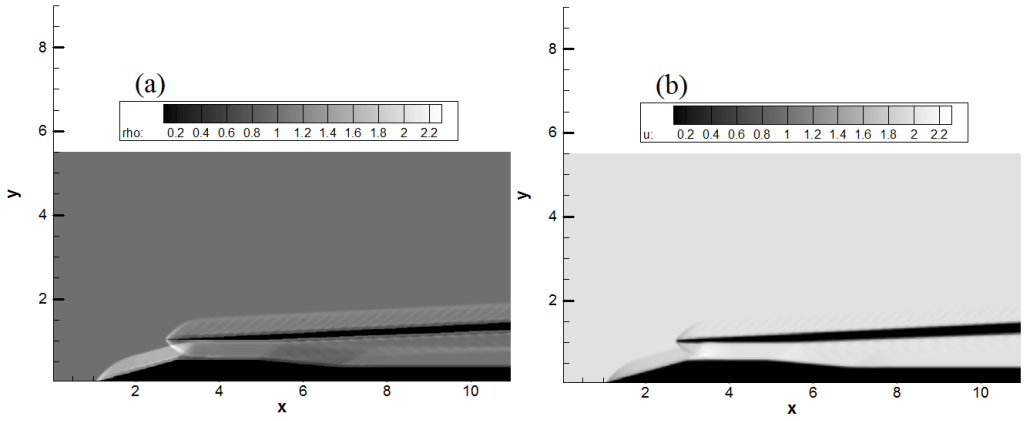

Figure 8. Distribution of (a): density and (b): horizontal velocity by the WNND scheme.

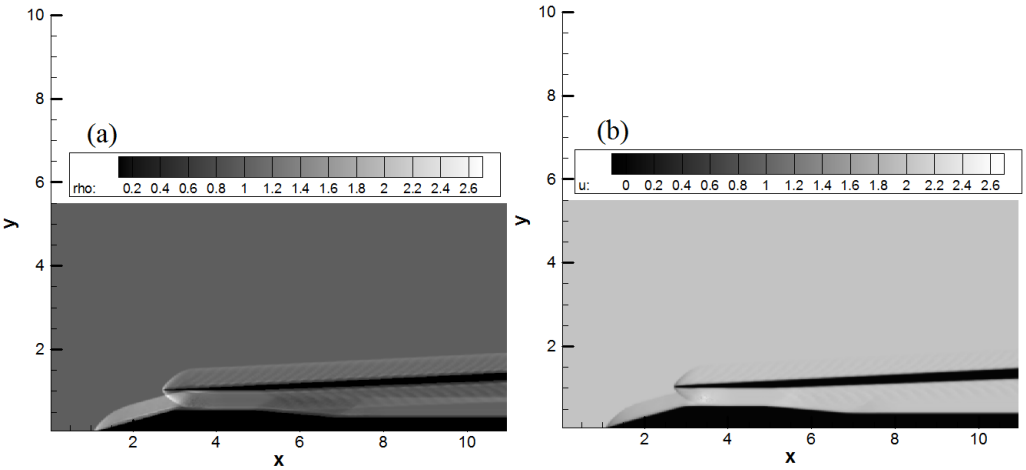

Figure 9. Distribution of (a): density and (b): horizontal velocity by the WENO scheme.

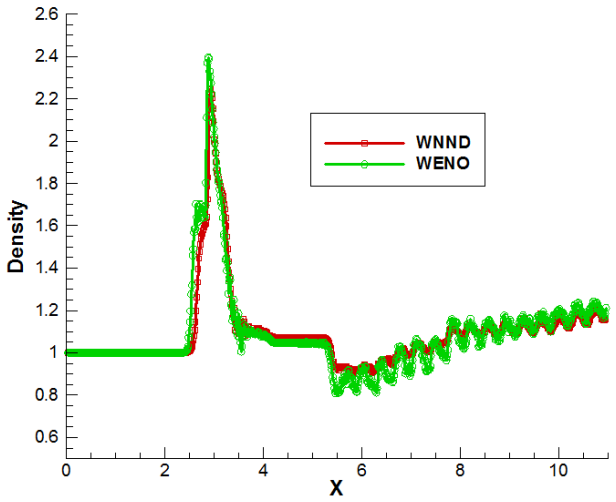

Figure 10. Comparison of density distribution along the line $y = 0.8$.

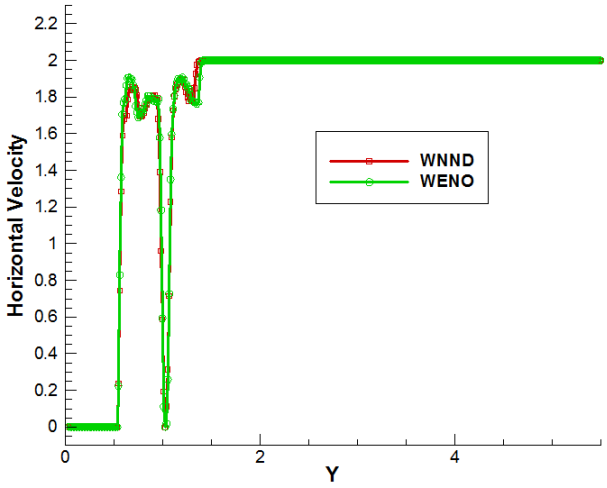

Figure 11. Comparison of horizontal velocity distribution along the line $x = 3$.

Figures 8 and 9 show the distribution of density and horizontal velocity for both schemes while the inlet operates at its supercritical regime which its main characteristic is the oblique shock train. It means that a considerable number of oblique shocks exist presenting a repetitive pattern of shock reflections. These oblique shocks are responsible for the compression needs to be achieved. Separations that occur cause the flow to distort.

According to Figure 10, the location of the shock is predicted to take place sooner by the WENO scheme. Point of maximum density is predicted higher by the WENO scheme while the region of highest density is somehow narrower. After the throat, the WNND scheme predicts higher values of density up to $x = 8$ while the trend reverses after this point and values predicted by the WENO schemes are higher. As observed in Figure 5, when the flow comes close to the cowl lip and passes through the throat area, a shock appears, and the density magnitude increases dramatically. Figure 11 shows a vertical distribution of the horizontal velocity at $x = 3$. Both schemes match well together particularly in regions where the values of horizontal velocity experiences ups and downs.

As it is evident from Figures 12 and 13, these two discretization schemes predict the flow qualitatively similar except for some differences regarding areas of maximum or minimum values. For example, the zone of maximum density at the interaction foot of two oblique shocks is larger in the WNND scheme. Generally, the WENO scheme predicts lower values with respect to the WNND scheme. Since the WENO scheme is of order 5, its computational requirement is higher, and it needs at least twice the time for each simulation.

Considering Figure 14, just when the flow approaches the throat, the interaction between the reflected shock from the cowl lip and the boundary layer causes the flow to separate. Downstream of the throat the flow accelerates again and reattaches to the body. The separation zone begins somehow sooner in the WENO scheme (separation point at about $x = 3$) while the flow begins to separate at $x = 3.15$ for the WNND scheme. The separation zone is larger in the WENO scheme with respect to the WNND scheme.

As it is evident from Figures 15 and 16, both schemes can capture the turning of velocity vectors correctly. According to Figure 15, velocity vectors turned their way upside before they reach the body since they are arrived at the shock front. When the flow reaches the cowl lip (Figure 16), another shock forces the velocity vectors to adapt their way according to the geometry. In addition, smaller velocity at the close vicinity of the surface is evident of the effects of the boundary layer which tries to zero the values of velocities.

Figures 17 and 18 verify that formation of the oblique shock and the angle at which it reflects are predicted correctly by both discretization schemes. Results of the study in Soltani et al. [9] are obtained by a mesh with 90000 elements while the current study is accomplished by a 180000-element mesh and it predicts the shock formation, its location, separation, and reattachment points correctly so the DDF LBM is a promising method in studying compressible flows while care should be taken in selecting the proper discretization scheme and simulation criteria regarding the CFL number. Since the WENO scheme is more vulnerable to instabilities regarding the CFL number and it takes a computational time at least twice the WNND scheme, authors recommend the WNND scheme for such problems.

Figure 19 shows the distribution of density along the line y=0.536814 where the outside wall of the cone exists. This figure illustrates how density peaks occur in different x stations. The first oblique shock which occurs in front of the cone tip causes density to experience a jump at around $x = 1.5$. Another jump in density occurs just before $x = 3$ where the cowl lip exists. Between $x = 3$ and $x = 3.5$ where the separation bubble dominates, density experiences a sharp decrease and then its value rises again. Further downstream, several minor peaks occur in density value due to successive oblique shocks. Except for the end part of the inlet, which has a straight shape, $8 < x < 11$, density values predicted by the WENO scheme are higher than those obtained by the WNND scheme. The conclusion is that

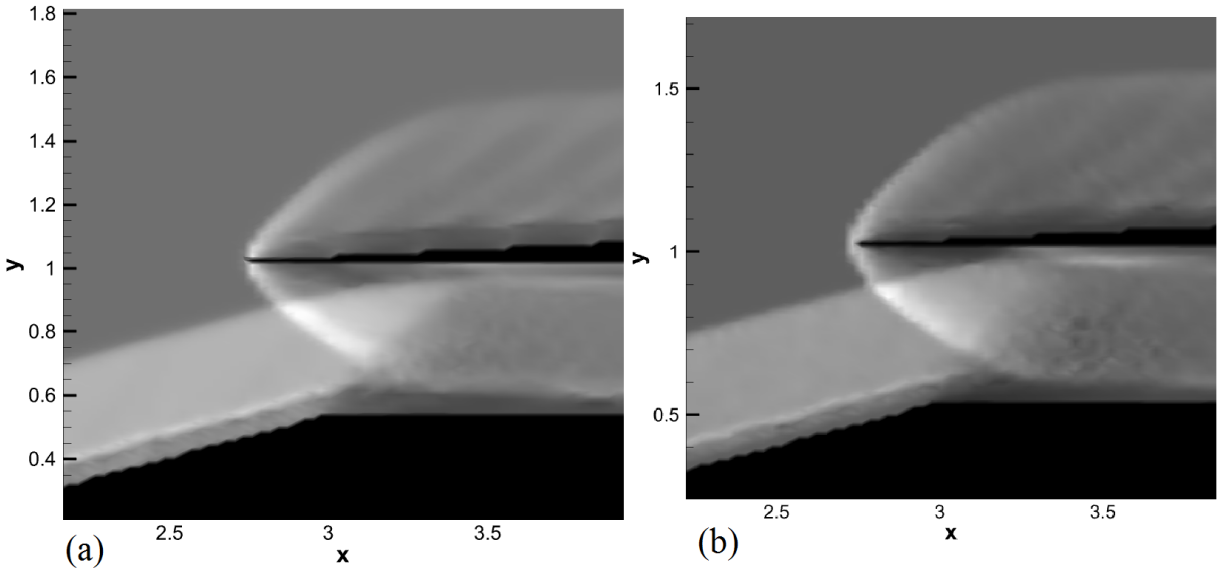

Figure 12. A magnified view of density distribution near the throat ((a): WNND, (b): WENO).

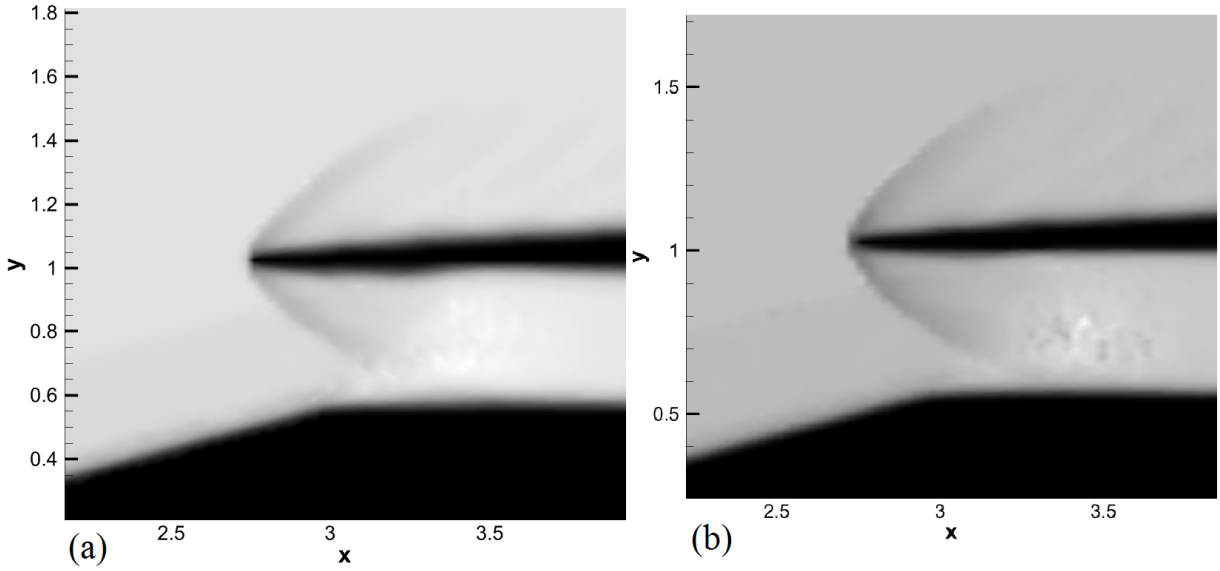

Figure 13. Magnified view of the Mach number distribution near the throat ((a): WNND, (b): WENO).

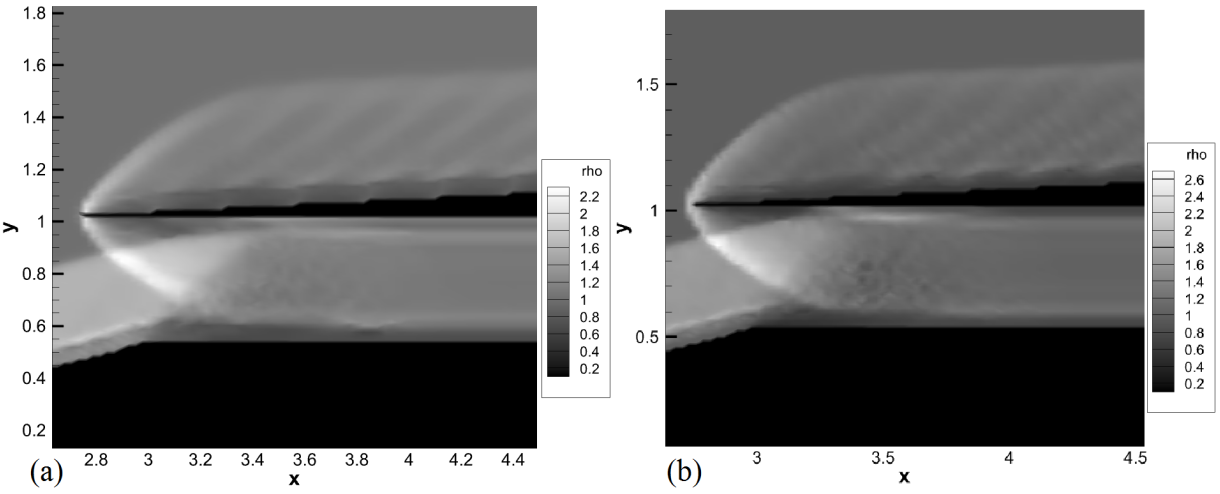

Figure 14. Comparison of discretization schemes regarding SWBLI ((a): WNND, (b): WENO).

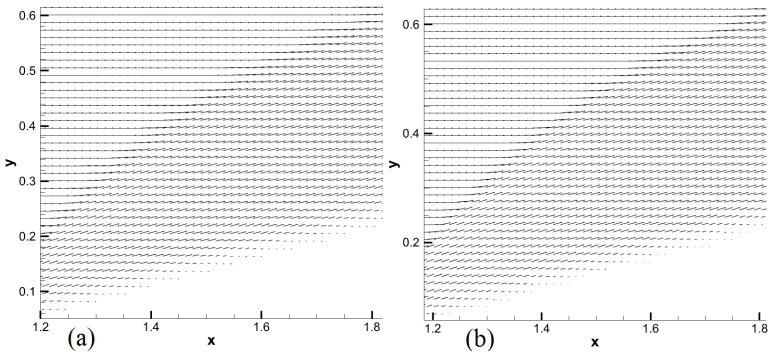

Figure 15. Velocity vectors at the beginning of the inlet (a): WNND, (b): WENO).

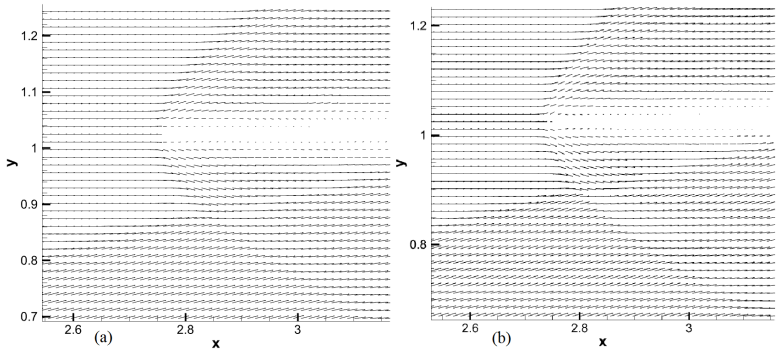

Figure 16. Velocity vectors at the proximity of the cowl lip (a): WNND, (b): WENO).

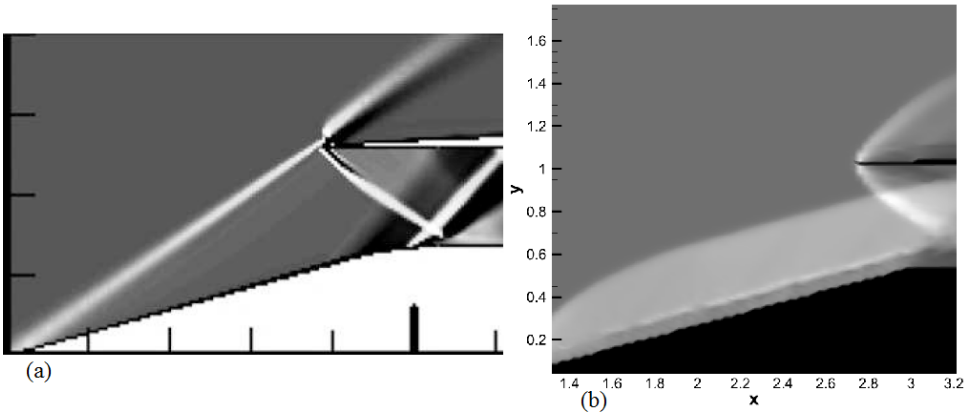

Figure 17. Comparison of density distribution (a): Soltani et al. [9], (b): WNND).

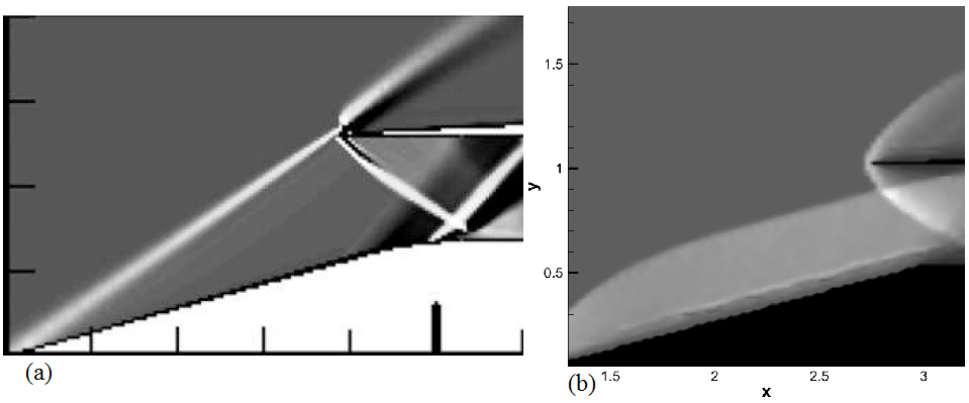

Figure 18. Comparison of density distribution (a): Soltani et al. [9], (b): WENO).

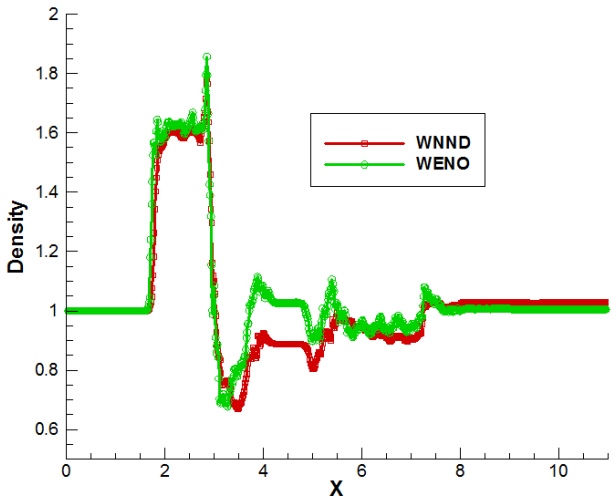

Figure 19. Density distribution at $y = 0.536814$.

the WENO scheme gives exaggerated results regarding values of macroscopic variables in compressible flows having shock waves.

5. Conclusion

In this study, two different spatial discretization schemes are employed to evaluate the effectiveness of a double distribution function lattice Boltzmann method (LBM) for analyzing shock wave-boundary layer interaction in a supersonic inlet. Specifically, the fifth-order WENO (Weighted Essentially Non-Oscillatory) scheme and the third-order WNND (Weighted Non-Negativity-Preserving Discretization) scheme are compared based on density and velocity distribution.

The WNND scheme, derived from the stencils of the NND scheme, operates as a third-order method. In contrast, the WENO scheme boasts a fifth-order accuracy but comes with a higher computational cost. Specifically, when simulating a supersonic inlet, the WENO scheme requires 1.3 to 1.5 times more computational time than the WNND scheme, depending on the mesh size. Although the WENO scheme is more accurate according to its higher order, it demands high memory usage, and it suffers from instability problems at higher CFL numbers compared to the WNND scheme. The WNND scheme, while computationally less intensive, preserves the essential physical aspects of the problem. Notably, in the WNND scheme, areas of maximum density at the point where two oblique shocks intersect are larger, whereas separation zones are more pronounced in the WENO scheme.

The strength of the double-distribution-function lattice Boltzmann method (DDF-LBM) lies in its ability to be executed on personal computer systems such as laptops. For this study, we employed a Core i7-10750H laptop with a 2.6 GHz CPU and 16 GB RAM. Remarkably, all runtimes remained within a single day (24 hours) for continuous simulations, whereas similar numerical simulations using ANSYS packages which solve the Navier-Stokes equations necessitated at least 3 days to achieve comparable results. Although compressible lattice Boltzmann methods, such as the double distribution function approach, hold promise for predicting discontinuities in high Mach number flows, further advancements are needed in exploring different discretization schemes and enhancing stability capabilities. In the context of compressible lattice Boltzmann methods, careful tuning, or adjustment of the CFL number is a crucial task since higher order discretization schemes reveal instabilities at some specific CFL numbers. According to the definition of the CFL number, the stability of the method is influenced by the minimum size used for space discretization. Therefore, careful consideration is necessary when selecting the minimum spatial step, as it directly impacts the time step. There is not a unique procedure to be prescribed for mesh resolution in such problems since flow instabilities may be triggered in any time so the selection criteria for simulation parameters such as the CFL number usually goes through a try and error process in order to find the optimum range.

Authors contributions
Both authors have participated equally and sufficiently in the intellectual content, conception and design of this research work or the analysis and interpretation of the data as well as the writing of the manuscript.

Availability of data and materials
No data was used for the research described in the article.

Conflict of interests
The author declare that they have no known competing financial interests or personal relationships that could have appeared to influence the work reported in this paper.

References

[1] D. S. Dolling. "Fifty years of shock-wave/boundary-layer interaction research: What next? ". *AIAA Jour-*

nal, **39**, 2001. DOI: https://doi.org/10.2514/3.14896.

[2] Q. Kun. "Development of lattice Boltzmann method for compressible flows.". *PhD dissertation, National University of Singapore*, , 2008. DOI: https://doi.org/10.1007/s11666-013-9904-0.

[3] A. G. Xu, G. C. Zhang, Y. B. Gan, F. Chen, and X. J. Yu. "Lattice Boltzmann modeling and simulation of compressible flows. ". *Front. Phys.*, **7**:582–600, 2012. DOI: https://doi.org/10.1007/s11467-012-0269-5.

[4] K. Li and C. Zhong. "A lattice Boltzmann model for simulation of compressible flows.". *International Journal for Numerical Methods in Fluids*, , 2014. DOI: https://doi.org/10.1002/fld.3984.

[5] Q. Li, Y. L. He, Y. Wang, and W. Q. Tao. "Coupled double-distribution-function lattice Boltzmann method for the compressible Navier-Stokes equations. ". *Physical review E*, **76**, 2007. DOI: https://doi.org/10.1103/physreve.76.056705.

[6] R. F. Qiu, Y. C. You, C. X. Zhu, and R. Q. Chen. "Lattice Boltzmann simulation for high-speed compressible viscous flows with a boundary layer. ". *Applied Mathematical Modeling*, **48**:567–583, 2017. DOI: https://doi.org/10.1016/j.apm.2017.03.016.

[7] A. Jammalamadaka, Y. Li, P. Gopalakrishnan, R. Zhang, and H. Chen. "Simulation of a canonical shock wave-boundary layer interaction using an LBM-VLES approach. ". *Aviation Forum, Fluid Dynamics Conference, June 25-29, Atlanta, Georgia*, , 2018. DOI: https://doi.org/10.2514/6.2018-4030.

[8] R. F. Qiu, H. H. Che, T. Zhou, J. F. Zhu, and Y. C. You. "Lattice Boltzmann simulation for unsteady shock wave/boundary layer interaction in a shock tube. ". *Computers and Mathematics with Applications*, , 2020. DOI: https://doi.org/10.1016/j.camwa.2020.07.012.

[9] M. R. Soltani, A. Daliri, and J. S. Younesi. "Effects of shock wave/boundary-layer interaction on performance and stability of a mixed-compression inlet. ". *Scientia Iranica*, **23**:1811–1825, 2016. DOI: https://doi.org/,10.24200/sci.2016.3928.

[10] C. Zhou, C. Zhong, K. Li, S. Xiong, X. Chen, and J. Cao. "Application of lattice Boltzmann method to simulation of compressible turbulent flow.". *Communications in Computational Physics*, **8**:1208–1223, 2010. DOI: https://doi.org/10.4208/cicp.300110.070510a.

[11] M. Hafez and E. Wahba. "Simulations of viscous transonic flow over lifting airfoils and wings. ". *Computers and Fluids*, **36**:39–52, 2007. DOI: https://doi.org/10.2514/6.2005-4802.